Journal of Manufacturing Processes 64 (2021) 606–619

Contents lists available at ScienceDirect

Journal of Manufacturing Processes

journal homepage: www.elsevier.com/locate/manpro

Cortical bone drilling: A time series experimental analysis of thermal characteristics

Shihao Li [a], Liming Shu [a,*], Toru Kizaki [a], Wei Bai [b], Makoto Terashima [c], Naohiko Sugita [a]

[a] Department of Mechanical Engineering, School of Engineering, The University of Tokyo, 7-3-1 Hongo, Bunkyo-ku, Tokyo, 113-8656, Japan
[b] State Key Laboratory of Digital Manufacturing Equipment and Technology, Huazhong University of Science and Technology, Wuhan, 430074, China
[c] TOKO Co., Ltd, 5-27-10, Hongo, Bunkyo-ku, Tokyo, 113-0033, Japan

ARTICLE INFO

Keywords:
Bone drilling
Thermal characteristics
Temperature distribution
Thermal image
Orthopedic surgery

ABSTRACT

Bone drilling is an essential and technically demanding procedure in many forms of surgery. The thermal characteristics in the drilling process directly affect thermal damage to the bone and postoperative recovery. In this study, a comprehensive experimental investigation was conducted to understand the thermal characteristics during cortical bone drilling using a bone cutting system coupled with a state-of-the-art infrared thermography and a dynamometer. The time-series temperature distributions, temperature history at different locations, and quasi-three-dimensional maximum temperature distributions were established and analyzed. The results show that the chisel edge, cutting lips, and margin are the main heat sources during bone drilling. The maximum temperature was generated by the cutting lip. Drilling in three feeding directions was performed to investigate the bone anisotropy. However, no sign of anisotropy on the temperature distribution was observed. But the maximum temperature and overheat duration exhibited a significant variation because of differences in the removal mechanism and bone density. Moreover, the effects of processing parameters on the thermal characteristics were analyzed in terms of the failure mechanism of bone. The drilling process duration may be the governing factor that can finally determine the thermal damage. This is the first study to reveal the thermal characteristics in full detail at the drill-exit with respect to the bone properties, processing parameters, drill-bit geometries, and inclined drilling. These results provide a fundamental understanding of the thermal characteristics in bone drilling and subsequently contribute to the formulation of various strategies for reducing the thermal damage to the bone.

1. Introduction

Bone is a natural composite with complex material property [1]. The drilling of bone performs a critical function in a wide range of surgeries, such as orthopedics and neurosurgery. Manual irrigation with sterile saline can increase the operation time and the risk of infection [2]; hence, many bone drilling processes are performed without irrigation. In the absence of a coolant, heat easily accumulates at the drilling site because of the relatively low thermal conductivity and specific heat capacity of the bone, increasing the risk of thermal osteonecrosis. Extensive research investigations have shown that thermal damage is caused by the combined effect of temperature elevation and thermal exposure time [3]. Eriksson et al. [4] suggested that the bone temperature should not exceed 47 ℃ for more than 60 s, indicating a relatively low thermal dose threshold. Moreover, the heat that accumulates with the increasing drilling depth may cause the most severe thermal damage to the end of the drill site and subsequently result in early aseptic loosening of the fixture [5]. Considering the complex thermal effects associated with postoperative recovery, gaining insight into the thermal characteristics during bone drilling is extremely important.

In previous decades, the parameters affecting the thermal characteristics during bone drilling have been investigated using various approaches, such as simulation, theoretical analysis, and experimental analysis. Tu et al. [6] and Sezek et al. [7] developed finite element (FE) models to investigate the effect of the processing parameters on the overheat zone in bone drilling. Fernandes et al. [8] developed a FE-based numerical model that incorporated the geometric, dynamic, and thermal characteristics to determine the thermo-mechanical stresses during bone drilling. However, it remains difficult to include the anisotropic and semi-brittle behaviors of the bone in the FE modeling. In

* Corresponding author.
E-mail address: l.shu@mfg.t.u-tokyo.ac.jp (L. Shu).

https://doi.org/10.1016/j.jmapro.2021.01.046
Received 26 October 2020; Received in revised form 10 January 2021; Accepted 30 January 2021
Available online 20 February 2021

contrast, Sui et al. [9] and Lee et al. [10] conducted leading works on developing theoretical models for predicting the temperature elevation in bone drilling. However, the mechanical interaction and heat transfer between the anisotropic bone and real drill bit geometry are yet to be considered. In summary, a considerable deviation remains between the predicted and experimental results because of model limitations.

Experimental analysis is considered the most reliable approach to investigate the thermal characteristics in bone drilling. Generally, there are two approaches for conducting the experiment—the use of thermocouples and the utilization of infrared thermography. In previous studies, thermocouples, as a contact type sensor, were most frequently used. The thermocouples were placed in pilot holes arranged according to a spacing order to investigate the thermal characteristics during bone drilling. However, the thermocouples can only be placed at a certain distance from the hole wall because of physical limitations, making it difficult to directly measure the temperature at the tool–bone interface. Moreover, the pilot hole creates an unnecessary interference to the heat dissipation in bone specimens, eventually influencing the temperature distribution around the drill site. In view of the foregoing limitations, many contradictory conclusions exist among the thermal studies on bone drilling. For instance, Karaca et al. [11] found that the temperature elevation decreased with the increase in spindle speed, whereas Sharawy et al. [12] presented an opposite conclusion. Considering these constraints, the sole utilization of thermocouples is a common but presumably insufficient approach for studying the thermal characteristics during bone drilling.

In comparison, infrared thermography provides a non-contact approach for measuring the temperature distribution in real time during bone drilling. The reliability of this technique has been evaluated in several studies by comparing the measurements obtained by the thermography and thermocouples in metal [13] and carbon fiber reinforced plastic drilling [14]. Thermography was utilized in bone machining to investigate the thermal effects of drill bits, surgical saws, and multi-grooved cutting tools in terms of processing parameters or material properties of the natural and synthetic bone, respectively [15–19]. The analyses were based on static temperature distributions because they always suffered from a low spatial resolution (>100 μm/pixel) and sampling rate (<100 Hz). Further analyses cannot be conducted because of the absence of post-processing. These limitations make it problematic to determine the most important details of the thermal characteristics associated with high-speed cutting. Consequently, gaining an accurate comprehension of the relationships between the thermal characteristics and parameters, such as the drill bit geometry, processing parameters, and bone properties, is hindered.

In this study, a comprehensive experimental investigation was conducted to understand the thermal characteristics during the cortical bone drilling using a bone cutting system coupled with a state-of-the-art infrared thermography and dynamometer. The time-series data recorded by the high-resolution infrared thermography were processed to obtain a quasi-3D temperature distribution in the vicinity of the drilling site for various analyses. To the authors' knowledge, this is the first study that determines the thermal characteristics at the drill exit in full detail with respect to the bone properties, processing parameters, drill-bit geometries, and inclined drilling. The derived results provide a fundamental comprehension of the parameters affecting the thermal effects in bone drilling and subsequently contribute to the formulation of various strategies for reducing the thermal damage during bone drilling.

2. Materials and methods

2.1. Experimental setup

The experimental setup is shown in Fig. 1. The five-axis horizontal machine center developed by the authors was used as the platform for conducting the drilling process. The temperature and force data were recorded by InfRec H9000 infrared thermography (Nippon Avionics Co., Ltd., Japan) and Kistler Dynamometer 9272 (Kistler Inc., Switzerland), respectively. An indium antimonide detector cooled by a Stirling cooling system was implemented to achieve highly accurate data with a 2% error range, a resolution of 0.025 °C at 30 °C, and a sampling rate of 200 Hz. Furthermore, a close-up lens with a spatial resolution of 15 μm was employed to optically enlarge the measuring area; the specifications of the imaging system are summarized in Table 1. Note that the drill bit temperature cannot be accurately measured because of the strong reflection caused by the smooth surface of the drill bits. Accordingly, this study mainly focuses on the bone at the drill exit plane. As was reported by Karmani et al. [20], and Eriksson et al. [4], irrigation by manual methods tends to have a limited cooling effect, which is, the coolant could hardly reach the tool-bone interface when drilling deep into the cortical bone and only the superficial tissue can be cooled.

Table 1
Specification of the imaging system.

Resolution	Sampling rate	Spatial resolution	Temperature range
640 pixels × 512 pixels	200 Hz	15 μm/pixel	0 to 150 °C

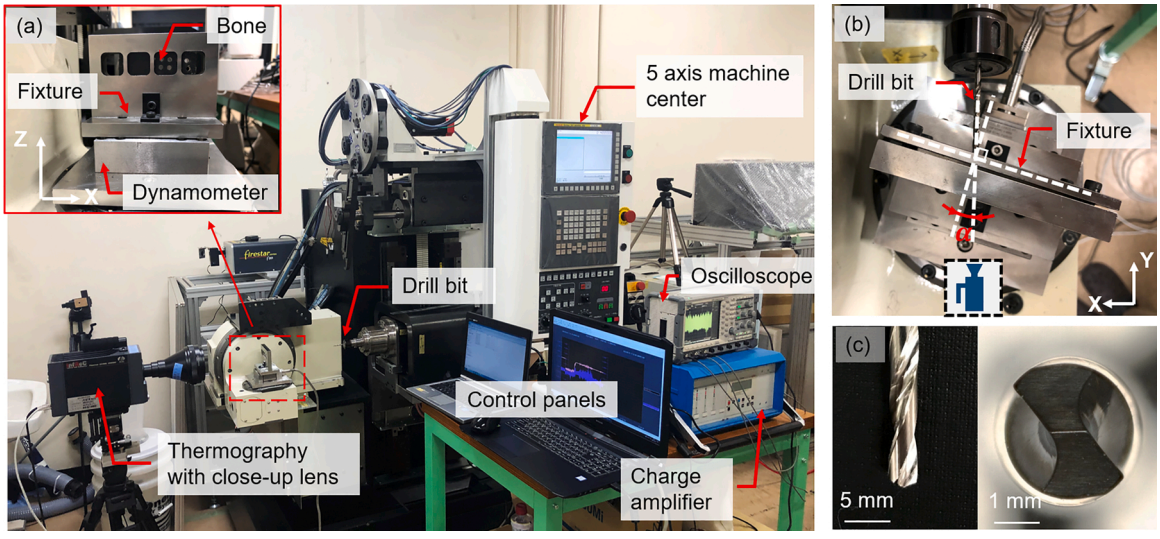

Fig. 1. (a) Experimental setup, (b) non-perpendicular drilling, and (c) drill bits.

Considering the potential ineffectiveness and uncertainty of the cooling effect, irrigation was not performed in the current experiments to achieve better observation.

2.2. Preparation of bone specimens

The cortical part of a fresh bovine femur was used in the experiment because it accurately resembles the human cortical bone in terms of material properties [18]; the detailed thermal properties are listed in Table 2. The cortical bone specimens were prepared along the axial and radial directions of the femur for investigating the effect of bone anisotropy on the temperature distribution, as shown in Fig. 2(a). All the specimens were obtained from the bone shaft and were milled to guarantee a smooth surface on the entrance and exit plane. The size of each specimen was approximately 60 mm (length) ×30 mm (width) with three different thicknesses (4, 6, and 8 mm). It should be noted that the thickness of specimens must be precisely controlled (error = ±0.05 mm) to eliminate the thickness-induced error in the temperature elevation. Test drilling was conducted on each specimen using certain processing parameters (i.e., 1000 rpm, 0.06 mm/rev) to determine if the specimen was aberrant by checking the drilling forces.

It is known that the emissivity can be affected by many factors and varies with the material. Moreover, the temperature measured by the thermography is a function of emissivity. Accordingly, the specimens were treated with a black-body spray (Tasco Co., Ltd., Japan) to achieve an emissivity of 0.94 on the drill exit plane [21].

2.3. Drill bit

A set of high-speed steel (JIS SKH51) drill bits produced by TOKO Co., Ltd. (Japan) is used to investigate the effect of drill bit geometry on the thermal characteristics in bone drilling, as shown in Fig. 1(c). The detailed geometrical parameters are listed in Table 3. Each drill bit was used up to a maximum of 10 times to eliminate the effect of tool wear.

2.4. Experimental procedure

The full factorial design of experiments was conducted to investigate the effect of bone thickness, drill bit diameter, and processing parameters on temperature elevation. It is also known that the cutting performance on the bone varies with the cutting direction with respect to the osteon direction [25]. Accordingly, the effect of drilling direction on temperature elevation was also investigated, as shown in Fig. 2(b). In some cases, surgeons have to drill in a non-perpendicular direction or on an uneven bone surface without any fixture. This would induce a significant lateral force and generate a considerable amount of frictional heat at the tool–bone interface, subsequently increasing the risk of thermal osteonecrosis. Therefore, the effect of tilt angle (α) (Fig. 1(b)) on the temperature elevation was also investigated in this study. It should be noted that no study on the thermal characteristics in non-perpendicular bone drilling has been conducted previously. All the experiments were repeated at least five times under each experimental condition. The statistical analyses of maximum temperature elevation and overheat (>47 °C) duration were implemented using the analysis of variance (ANOVA). The experimental conditions are shown in Table 4.

Table 2
Thermal properties of the cortical bone, drill bit, and air.

Material property	Bovine cortical bone [22]	High-speed steel (Material of drill bit) [23]	Air at 27 °C [24]
Density (kg/m3)	1640	8060	1.16
Elastic modulus (MPa)	16,700	193,000	–
Specific heat (J/kg)	1640	500	1007
Thermal conductivity (W/mK)	0.58 (Longitudinal) 0.53 (Circumferential) 0.54 (Radial)	16.2	0.026
Thermal diffusivity (mm^2/s)	2.38e-7	2.73e-5	2.25e-5

2.5. Thermal data postprocessing

In Fig. 3, the workflow of data processing is illustrated. All the processes were performed by Python scripts. The time-series thermal data were first extracted from raw data. The hole wall was identified based on the Hough circle transform [26]. To obtain the temperature history at a certain distance from the hole wall, the time series of instantaneous temperatures at the corresponding position were extracted. These temperature histories were then processed in two ways: the circular walls of temperature histories were unfolded to perceive the thermal characteristics directly and the mean temperature history curves were constructed by averaging the temperatures in the sampling circles following a certain chronological order. The confidence interval of the mean temperature process was set to 95 % to reduce the data random error. The line width of the extracted circle was set as 2 pixels (30 μm) to improve the accuracy. The maximum temperature and corresponding time point at each pixel were extracted to obtain the quasi-3D temperature distribution.

3. Results

3.1. Temperature distribution along drilling direction

The temperature distribution along the drilling direction was investigated to understand the effect of drilling depth on thermal characteristics. The thermography is placed perpendicular to the drilling direction, as shown in Fig. 4. It should be noticed that the heat transfer here is supposed to be different from normal cases because there is only an ultra-thin layer of bone between the drilling site and specimen periphery (i.e., observation surface). The minimum distance between the observation surface and hole wall was 0.1 mm. It is evident that the maximum temperature increased with the drilling depth, which was also reported in previous studies [8,18,24]. As drilling began and the drill bit gradually entered the specimen, the maximum temperature sharply increased at a drilling depth of 0–1 mm. Another rapid increase was observed at the end (7–8 mm) of drilling. This can be explained by the increasing resistance in evacuating chips with increasing cutting depth, which produces considerably more frictional heat, thus causing a sharp increase in temperature. Overall, the maximum temperature increased with the drilling depth and peaked at the drill exit surface. Accordingly, this study mainly focused on the temperature characteristics of the drill exit surface.

3.2. Analysis of thermal characteristics on the drill exit surface

The variation of the thrust force as a function of drilling depth and the corresponding sketch at different critical drilling depths are shown in Fig. 5. The drill exit plane and drilling depth are defined as the reference plane and the distance between the chisel edge and reference plane, respectively. Three typical stages are defined and analyzed in detail: Stage 1 (S1), the period before the chisel edge penetrates the drill exit plane; Stage 2 (S2), the period between the time point of chisel edge penetration and the time point when the entire cutting lips penetrate the drill exit plane; Stage 3 (S3), the period after the cutting lips pass the drill exit plane. The corresponding thermal images on the drill exit surface in each stage are shown in Fig. 6. The thermal characteristics of the entire drilling process were further investigated through postprocessing.

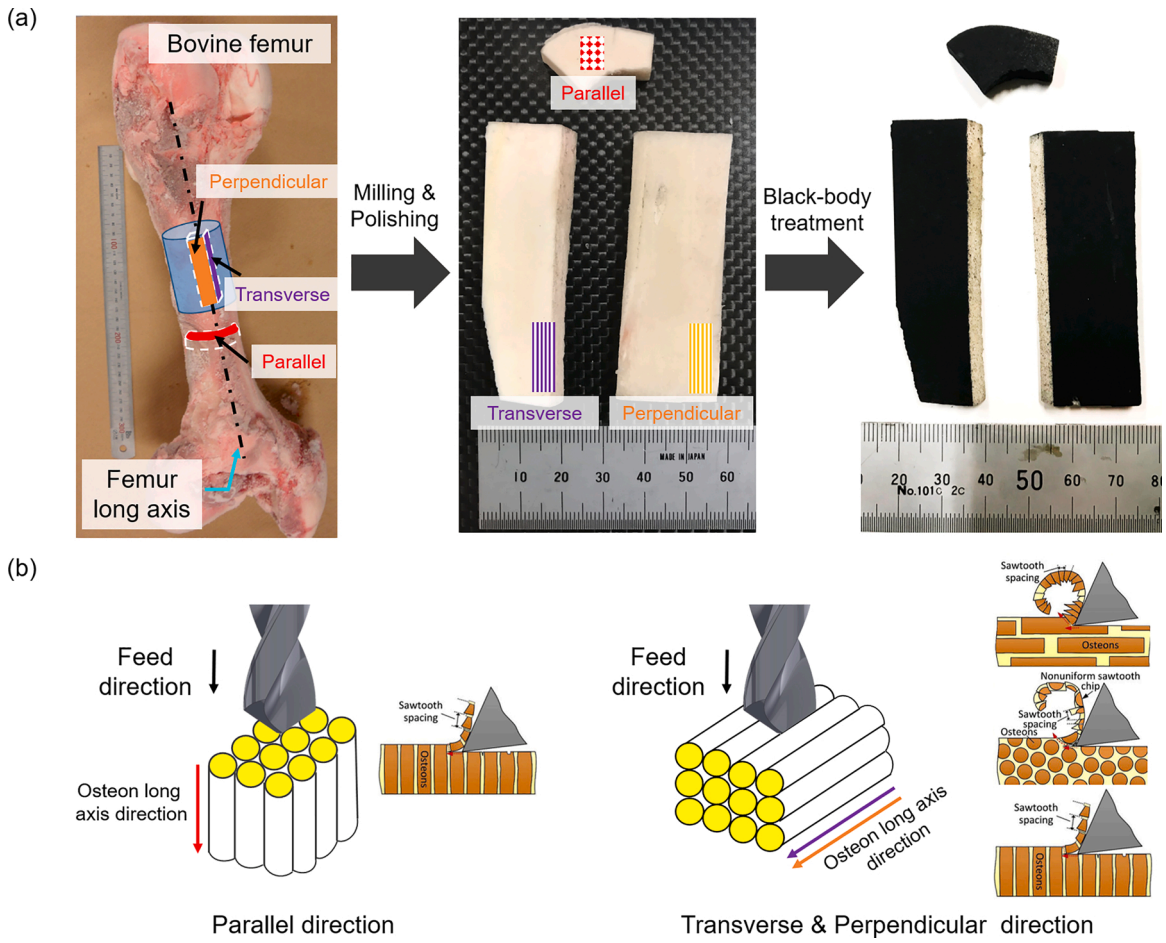

Fig. 2. (a) Preparation of specimen and (b) drilling directions relative to osteon direction.

Table 3
The geometry of the drill bit.

Diameter (mm)	Point angle (°)	Helix angle (°)	Margin width (mm)	Chisel edge angle (°)	Length of chisel edge (mm)
2.5	118	29	0.225	125	0.44
3.2	118	29	0.25	125	0.64
4.2	118	29	0.32	125	0.84

Table 4
Experimental conditions.

Items	Parameters
Workpiece	Cortical part of bovine femur
Thickness (mm)	4, 6, 8
Drilling direction	Parallel, Transverse, Perpendicular
Drill bit diameter (mm)	2.5, 3.2, 4.2
Point angle (°)	118
Spindle speed (rpm)	500, 1000, 1500, 2000,2500
Feed rate (mm/rev)	0.02, 0.04, 0.06, 0.08, 0.1
Tilt angle (°)	0, 3, 6, 9, 12, 15
Environment temperature (°C)	23

3.2.1. Temperature distribution and mechanical damage reflecting the tool-bone interaction

The temperature distribution at the end of S1 is illustrated in Fig. 6 (a). The temperature is evenly distributed in each direction with a peak of 60.3 °C at the center. The temperature rapidly increased from 60.3–78.4 °C in less than 0.01 s as the chisel edge penetrated the drill exit surface (Fig. 6(b)) possibly because of bone delamination. The delamination is caused by the thrust force against the last layer of bone, negating effective cutting by weakening the contact between the tool and bone. Considering the relatively short period of weak contact and the low thermal conductivity of the bone, the two main heat sources (i.e., conductive heat and frictional heat) were not sufficiently intense to increase the bone temperature to the same level as the bone being cut. At the start of S2, the heat generated by the cutting lips became the main heat source on the drill exit plane (Fig. 6(c)). As shown by the enlarged image of S2, the temperature of the zone behind the cutting lip was significantly higher than that at the uncut zone. At the end of S2, most of the bone material inside the hole wall was removed, exposing the entire cutting lip (Fig. 6(d)). The heat source was evidently at the interface between the cutting lip and bone as shown in the enlarged image of S3. The heat was first generated at the cutting lip (82.5 °C) and then peaked immediately behind it (92.1 °C) because of heat accumulation. In S3, the margin friction became the main heat source, as shown in Fig. 3(e). The temperature dropped from 92.5–71.3 °C at the tool–bone interface, indicating that the heat generated at this stage was lower than that in S2. After the retraction of the drill bit, the heat source at the drill exit plane ceased, resulting in a rapid decrease in temperature (Fig. 6(f)). The surface electron micrographs (SEM) were shown in Fig. 6(g, h). Delamination and micro cracks were found on the drill-exit and the hole wall, respectively.

3.2.2. Historical temperature variation on the drill exit surface

The temperature in the vicinity of the drill site is the key to determining the level of heat-induced damage to the bone. The temperature history at different distances from the hole wall is presented in Fig. 7.

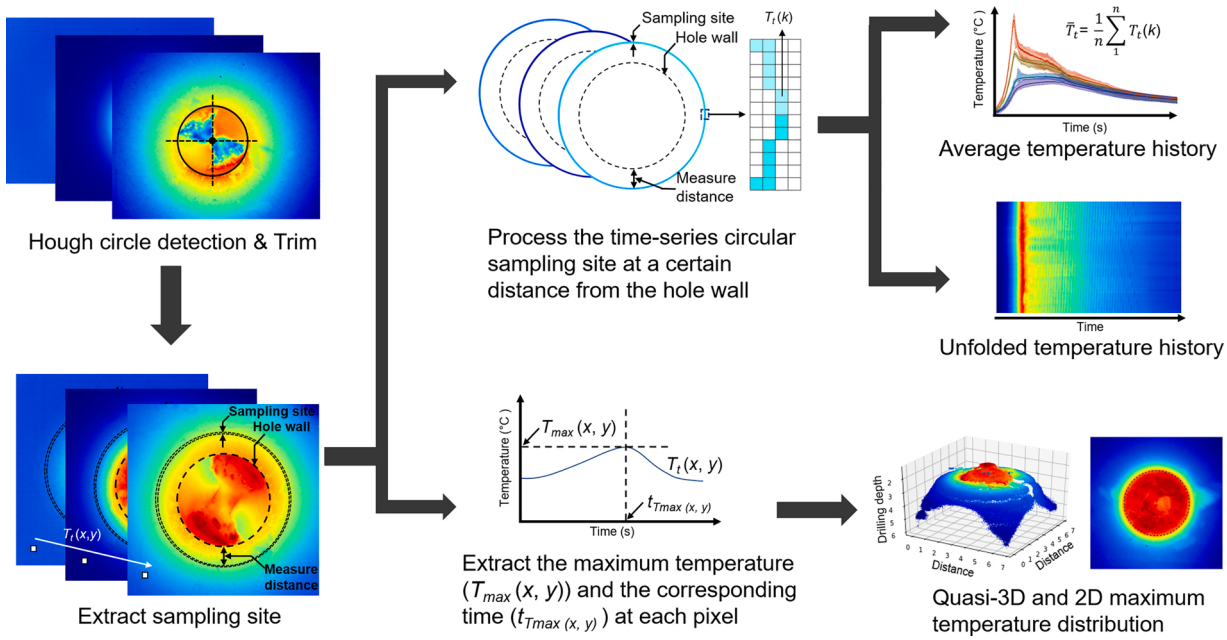

Fig. 3. Data processing workflow.

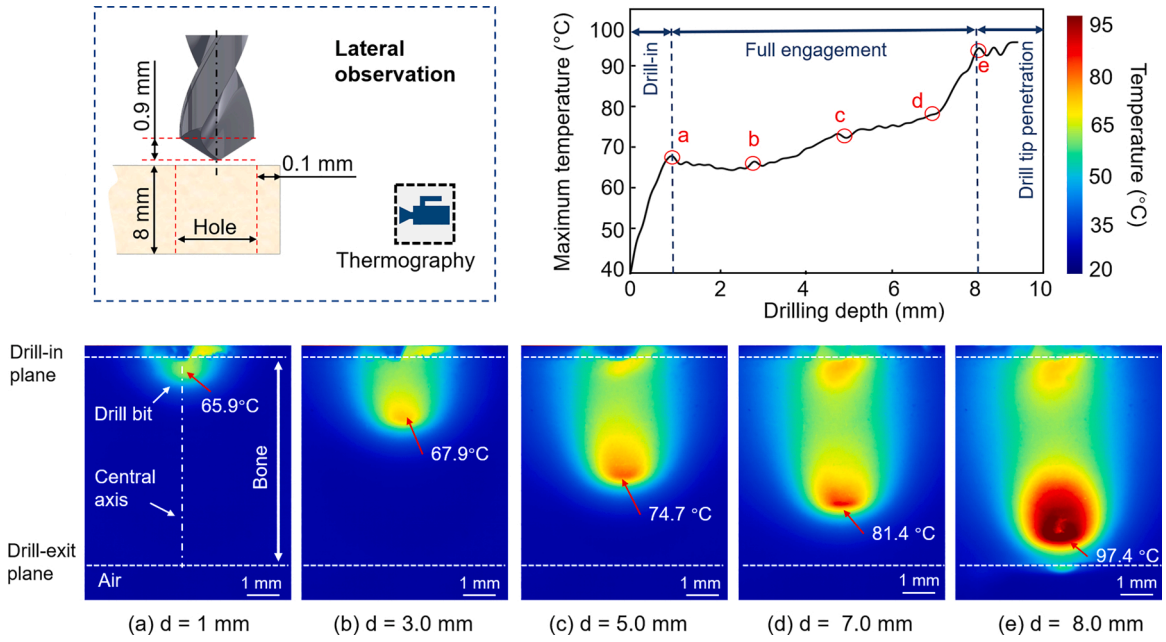

Fig. 4. (a) Maximum temperature variation and (b) time series distribution (bone thickness: 8 mm; perpendicular direction, 500 rpm, 0.06 mm/rev).

Four circular sampling sites at different distances (0, 0.3, 0.75, and 1 mm) from the hole wall are marked in Fig. 7(a). The average temperature histories with envelopes are shown in Fig. 7(b). The envelope is the instantaneous temperature range at the circular sampling site. The corresponding unfolded temperature histories at each distance from the hole wall are shown in Fig. 7(c–e). Based on the temperature histories (Fig. 7(b–e)), the characteristics of temperature elevation are found to be highly dependent on the distance from the hole wall. The temperature history at nearer distances (0 and 0.3 mm) peaked at the end of S2 and then rapidly decreased. The peak of the temperature histories at more distant locations (0.75 and 1.0 mm) remained for several seconds. The temperature histories at the 0 and 0.3 mm distances exceeded the suggested threshold of 47 °C for approximately 10 s. The temperature histories at distances of 0.75 and 1.0 mm did not exceed 47 °C during the entire process.

In Fig. 8, the two-dimensional (2D) and quasi-3D maximum temperature distribution are presented. The 2D temperature distribution image is the top view of the quasi-3D distribution. The area between 0.0 and 0.49 mm from the hole wall, where the maximum temperature exceeded 47 °C, is determined as the thermal damage risk zone, as shown in Fig. 8(a). The area near the hole wall sustained the most severe thermal damage in the entire process. As shown in Fig. 8(b), the bone temperature in the vicinity of the drill site peaked at the end of S2, and a distinct time delay in reaching the maximum temperature of the bone at a more distant position was observed.

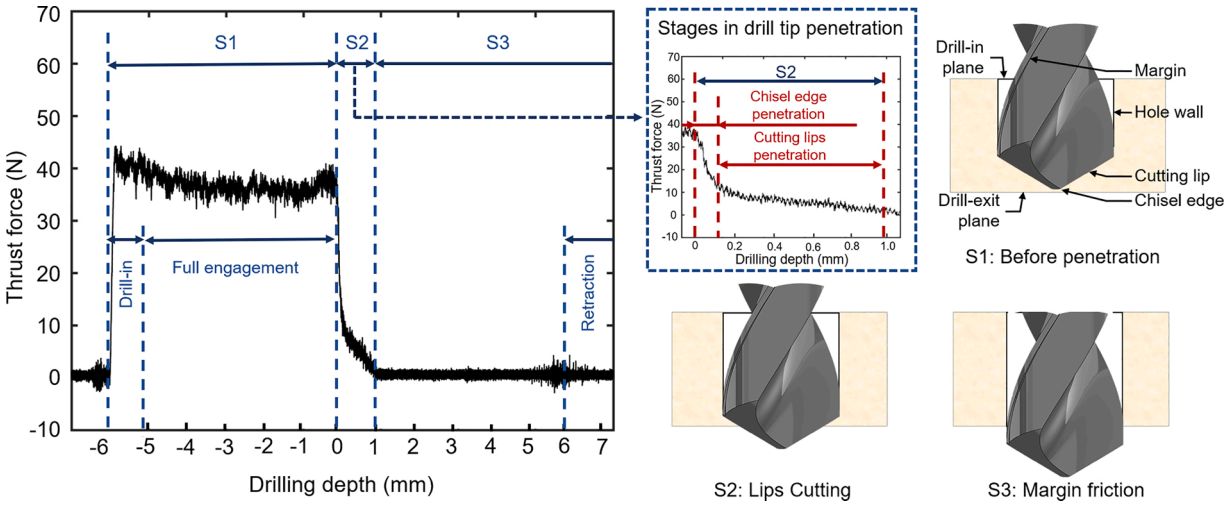

Fig. 5. (a) Variation of thrust force and (b) corresponding schematic (perpendicular direction, 1000 rpm, 0.06 mm/rev).

3.3. Effect of feeding direction and bone thickness on temperature elevation

It is known that the cutting performance in orthogonal bone cutting is significantly dependent on the cutting direction [25]. The unfolded temperature histories and mean maximum temperature of different feeding directions are presented in Fig. 9. It should be noted that the cutting mechanisms in the perpendicular and transverse feeding directions are equivalent because of the rotational symmetry of the drill bits, as shown in Fig. 2. Thus, the unfolded temperature histories along the parallel and perpendicular directions are shown in Fig. 9. Among the three feeding directions, no temperature distribution anisotropy was observed, whereas significant differences among the average maximum temperatures (T_{max}) and overheating durations (t_{over}) were found. The temperature elevation in the perpendicular drilling direction was considerably higher than those in the other two directions. Drill-exit and the hole wall SEM of the transverse direction and parallel direction drilling are shown in Fig. 9(e, f). Moderate delamination and micro crack were found in transverse drilling. Meanwhile, the parallel drilling exhibited little delamination and mild micro crack.

The mean temperature histories obtained by the experiments performed on bone samples with different thicknesses at 0 and 0.3 mm distances from the hole wall are shown in Fig. 10. It can be observed that the maximum temperature significantly increased with the bone thickness, which is consistent with the lateral observation shown in Fig. 4. Further, when the bone thickness was less than 4 mm, the size of the overheat zone was negligible.

3.4. Effect of drill bit diameter on temperature elevation

Fig. 11 shows the average temperature histories obtained by the experiments performed using 2.5, 3.2, and 4.2 mm drill bits at distances of 0 and 0.3 mm from the hole wall. The highest temperature elevation (82.3 °C), achieved by the 3.2 mm drill bit, was approximately 10 and 21 °C higher than those of the 2.5 and 4.2 mm drill bits, respectively. The overheat time of the 3.2 mm drill bit at a distance of 0.3 mm from the hole wall was approximately 4 s; the maximum temperatures reached by the 2.5 and 4.2 mm drill bits at a distance of 0.3 mm did not exceed 47 °C.

3.5. Effect of processing parameters on temperature elevation

The thermal data at 0.3 mm from the hole wall were used to accurately reflect the maximum temperature (T_{max}) and overheat duration (t_{over}) of the bone in the vicinity of the drill site. The confidence level of the data was first examined. The parameter combinations of feed rate (f) and spindle speed (n) and the corresponding outputs (i.e., T_{max} and t_{over}) is shown in Table 5. The contributions of the processing parameters were obtained with ANOVA, as shown in Tables 6 and 7. The spindle speed and the feed rate (feed per revolution) contributed to T_{max} and t_{over} the most, respectively.

To investigate the effect of f and n on the average T_{max} and t_{over}, the T_{max} and t_{over} data were processed by third-order polynomial curve fitting to obtain the fitting surface, as shown in Fig. 12. The R^2 values were 0.80 and 0.95, respectively. Both T_{max} and t_{over} exhibited a declining trend with increasing f; however, t_{over} decreased with n, whereas T_{max} increased with n.

3.6. Effect of inclined drilling on temperature elevation

In some cases, surgeons have to drill in a non-perpendicular direction or on an uneven bone surface without any fixture. This would induce a significant lateral force, thus generating considerable frictional heat at the tool–bone interface and subsequently increasing the risk of thermal osteonecrosis. Thus, the effect of tilt angle (α) (Fig. 13(f)) on temperature elevation was also investigated in this study.

The temperature distribution at each stage in a 9° inclined drilling is presented in Fig. 13(a–d). An asymmetric heating effect is caused by the lateral force-induced frictional heat, resulting in considerably higher temperature distribution on the left side of the hole wall. The maximum temperature distribution and overheat zone ($T_{max} > 47$ °C) are shown in Fig. 13, (e) and (g), respectively. To understand the effect of lateral force on the asymmetric heating, the total overheat zone ($S_{over\text{-}all}$) was divided into left ($S_{over\text{-}left}$) and right ($S_{over\text{-}right}$) overheat zones by the Y axis. The $S_{over\text{-}all}$ and $S_{over\text{-}right}$ increased with the tilt angle, while $S_{over\text{-}left}$ first increased and then decreased with the tilt angle, as shown in Fig. 13(h). Moreover, T_{max} and t_{over} first sharply increased and then slightly changed with the increasing tilt angle (Fig. 14).

4. Discussion

To the best of the authors' knowledge, this is the first study that reports on the thermal characteristics at the drill exit in full detail with respect to the feeding direction, drill bit diameter, processing parameters, and inclined drilling. This can aid in establishing a fundamental understanding of the parameters affecting the thermal effects. Based on the foregoing, various strategies for reducing thermal damage during bone drilling are subsequently proposed.

As shown in Figs. 4 and 8, the temperature elevation is highly dependent on the drilling depth and distance from the cutting area,

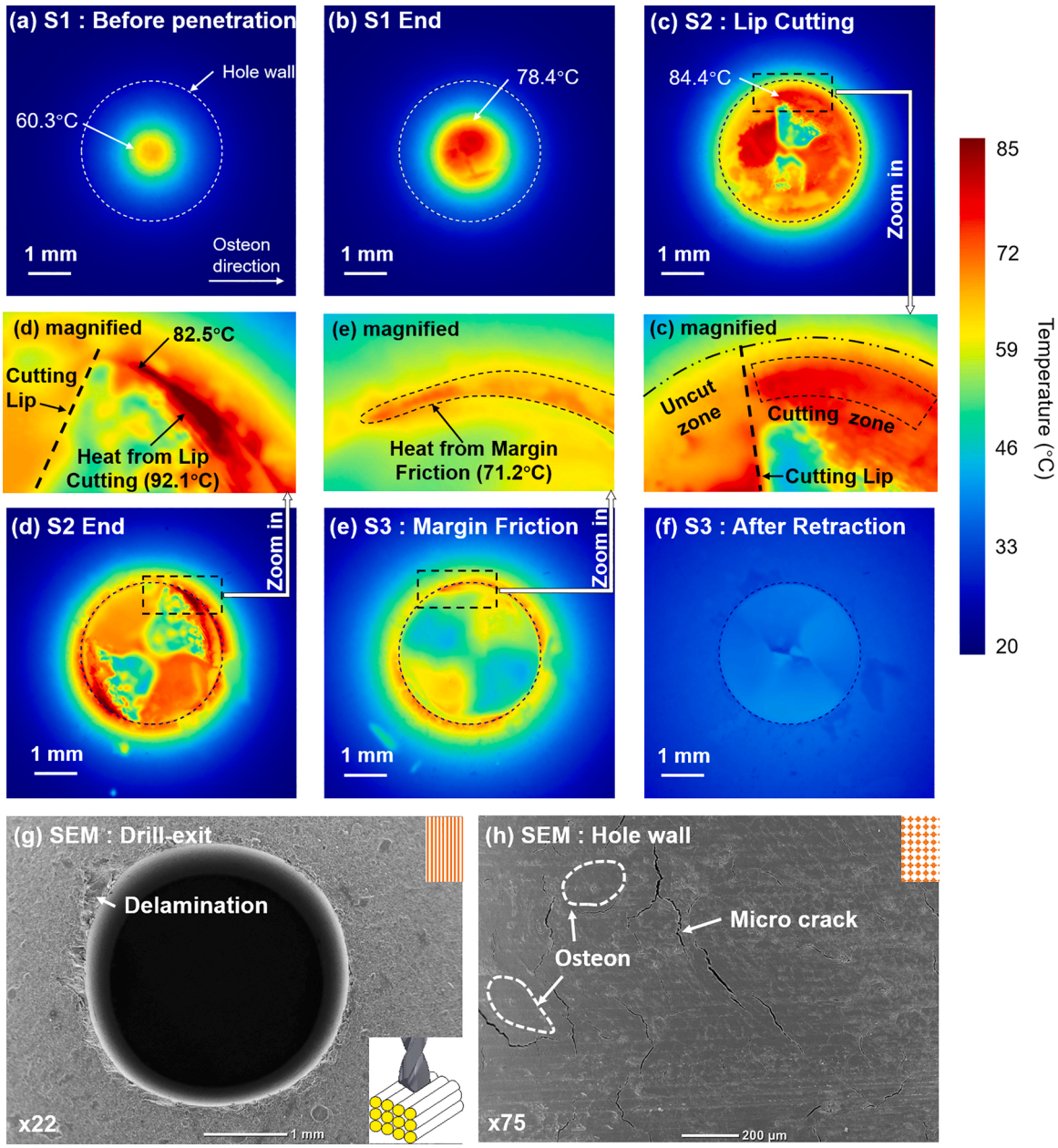

Fig. 6. (a-f) Time series temperature distribution (perpendicular direction, 500 rpm, 0.06 mm/rev) and (g, h) SEM of the drill-exit and the hole wall.

which is also supported by the immunohistochemistry investigation conducted by E.B. Dolan et al. [29]. Thermocouples were utilized to investigate the temperature elevation in bone drilling [24,30–32]; the distances between the sampling sites and cutting area were basically larger than 0.5 mm. In some cases, the drilling depth was also not precisely controlled [11]. These deficiencies are the possible reasons for the contradictory conclusions reached by previous studies on the thermal effects in bone drilling.

The detailed thermal characteristics on the drill exit surface during the bone drilling are presented in Figs. 6 and 7. Contrary to expectations, although a considerable amount of heat was generated by the chisel edge cutting, the bone outside the hole was practically unaffected during the S1 stage. This was mainly because of the relatively low thermal conductivity of the cortical bone, as summarized in Table 2. The heat generated in the S1 stage forms the temperature base of the drilling process. The maximum temperature elevation in the tissue in close proximity to the hole wall occurred at the end of the lip cutting stage, S2, significantly affecting the total temperature elevation in more distant areas. From Fig. 7, it can be concluded that although the duration of S2 only accounts for a small proportion of the entire process, the heat generated in S2 together with S1 performs a determinant role in the maximum temperature elevation in most areas. With regard to the margin friction stage (S3), it is found that the frictional heat generated during this stage can retard or even halt the temperature decrease at a certain value exceeding the thermal threshold. Thus, it can be concluded that the thermal exposure duration is mainly determined by the S3.

The cortical bone is an anisotropic material in terms of the removal mechanism. It is known that in cortical bone drilling, the removal mechanism of osteons varies with the rotation of drill bits. When drilling is performed in the transverse and perpendicular directions, the osteon removal mechanism is a mixed model of across, transverse, and parallel cutting. In the parallel feeding direction, the sole osteon removal mechanism is transverse cutting. As shown in Fig. 9, (a) and (b), no anisotropy in the temperature distribution in both feeding directions is observed, and T_{max} and t_{over} exhibit significant differences among the three feeding directions (Fig. 9(c)). This result may be explained by the

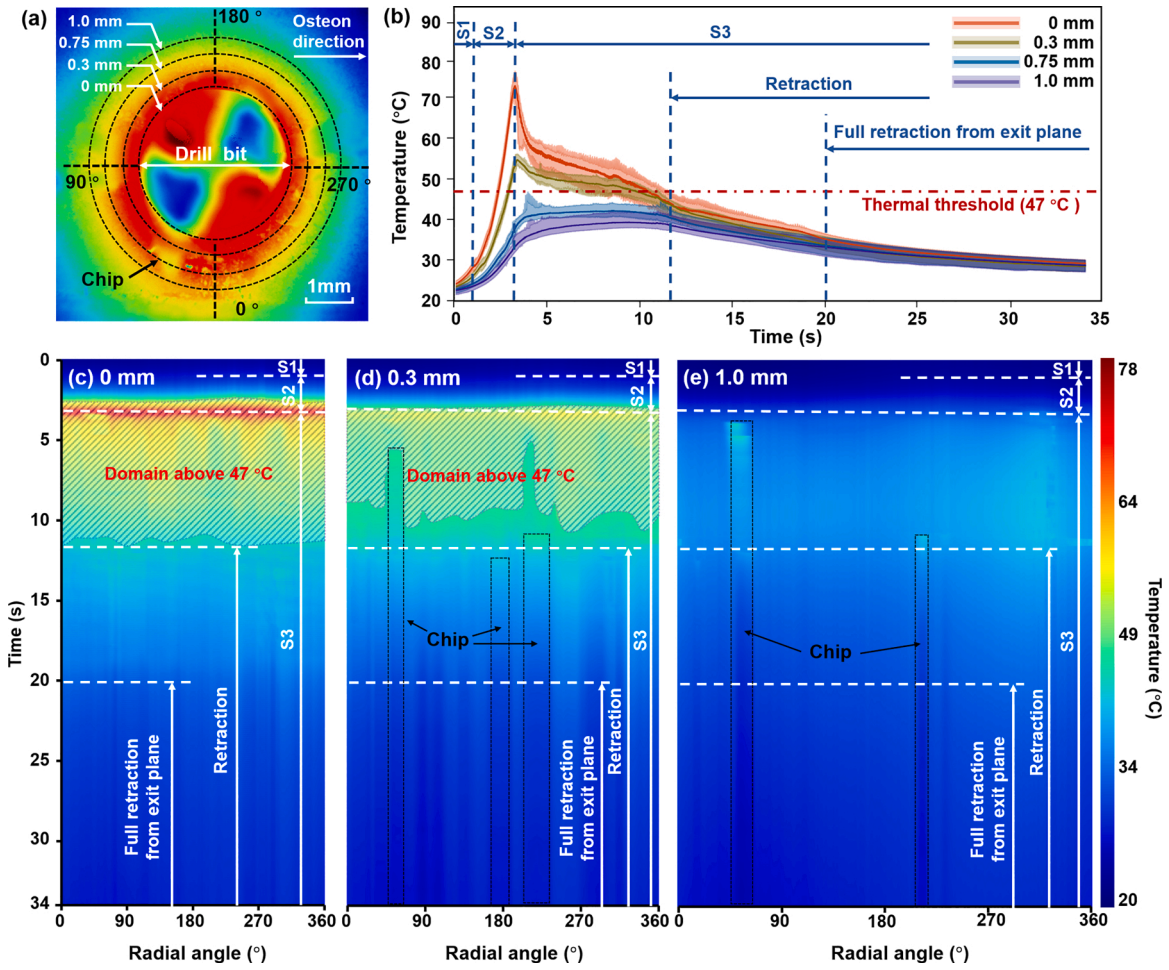

Fig. 7. Temperature histories at various distances from hole wall. (perpendicular direction, 500 rpm, 0.06 mm/rev).

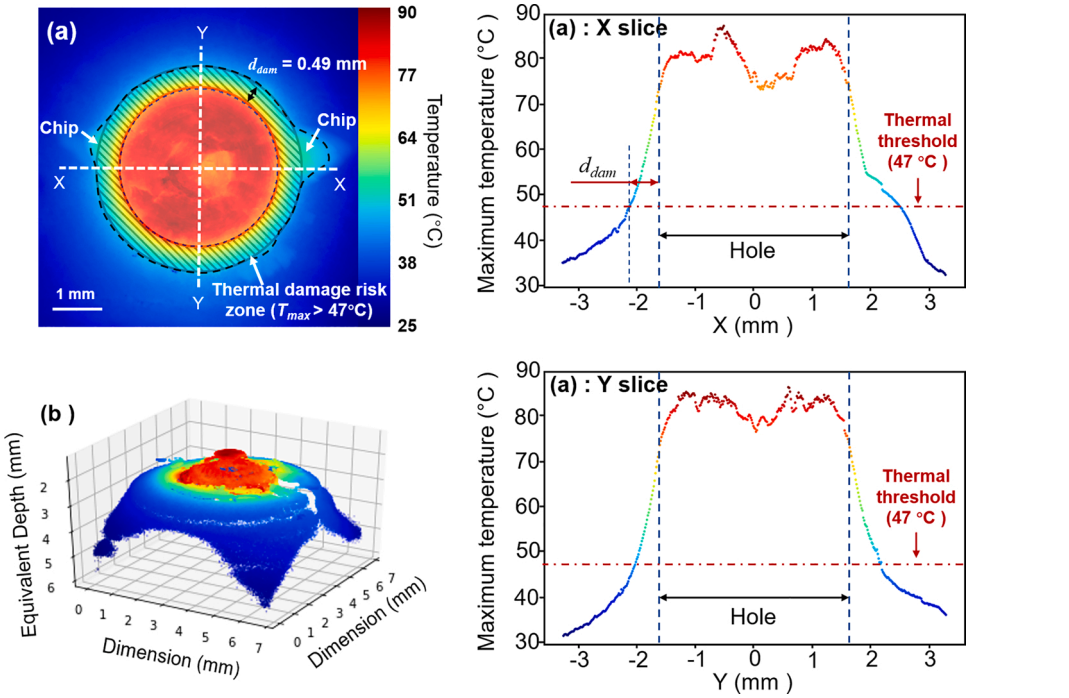

Fig. 8. (a) 2D and (b) quasi-3D maximum temperature distribution. (perpendicular direction, 500 rpm, 0.06 mm/rev).

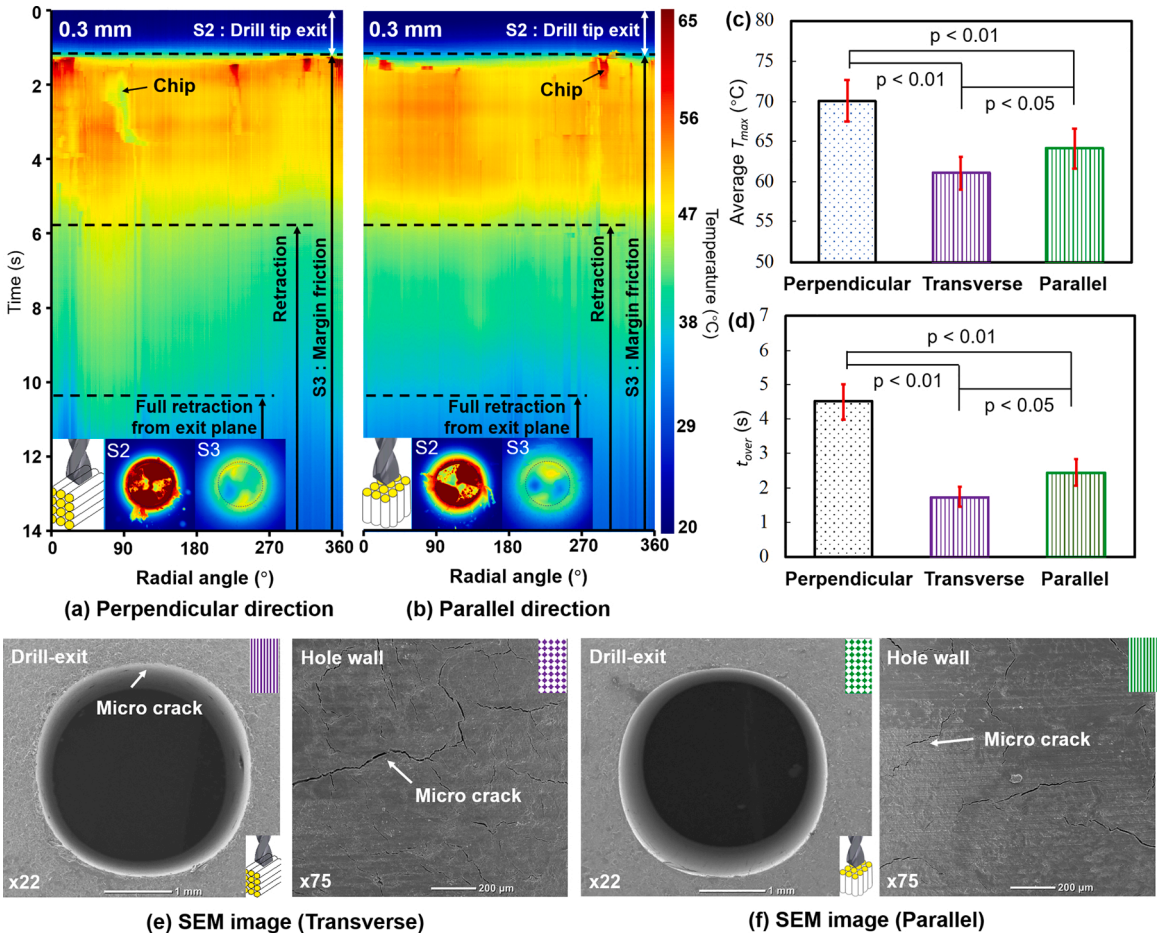

Fig. 9. (a) Perpendicular drilling direction and (b) parallel drilling direction temperature histories; (c, d) Comparison of average maximum temperatures among three drilling directions at 0.3 mm from the hole wall. (1000 rpm, 0.06 mm/rev); (e, f) Drill-exit and the hole wall SEM of the transverse direction and parallel direction drilling.

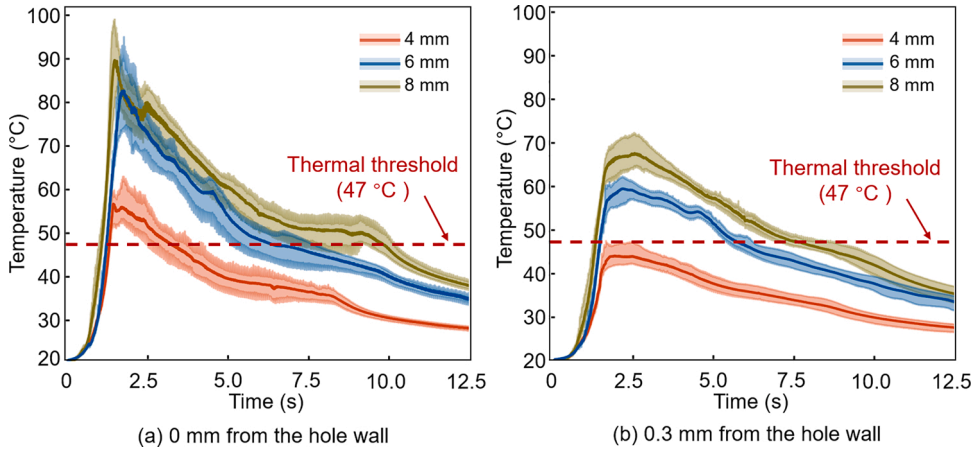

Fig. 10. Temperature histories of different bone thicknesses at 0 and 0.3 mm from the hole wall (Perpendicular direction, 1000 rpm, 0.06 mm/rev).

combined effect of the bone osteon removal mechanism and bone density. Generally, the cortical bone density decreases from the outer part to the inner part along the radial direction [33]. During drilling, the bone with a higher density could cause a higher heat generation [24]. In this study, although the osteon removal mechanisms of the transverse and perpendicular feeding directions are equivalent, the transverse feeding did not have to cut through the densest surface part, resulting in a lower temperature elevation. Similarly, although the specific cutting energy in the parallel feeding (i.e., transverse cutting) direction is the highest in terms of osteon removal mechanisms, the lower bone density at the drilling site relative to the perpendicular direction results in a lower temperature elevation. The variation in mechanical damage of the three feeding directions is also thought to be caused by the aforementioned differences in material property. As shown in Fig. 6(g, h) and Fig. 9(e, f), the perpendicular and transverse feeding direction both exhibited delamination and micro cracks, while only mild micro cracks happened

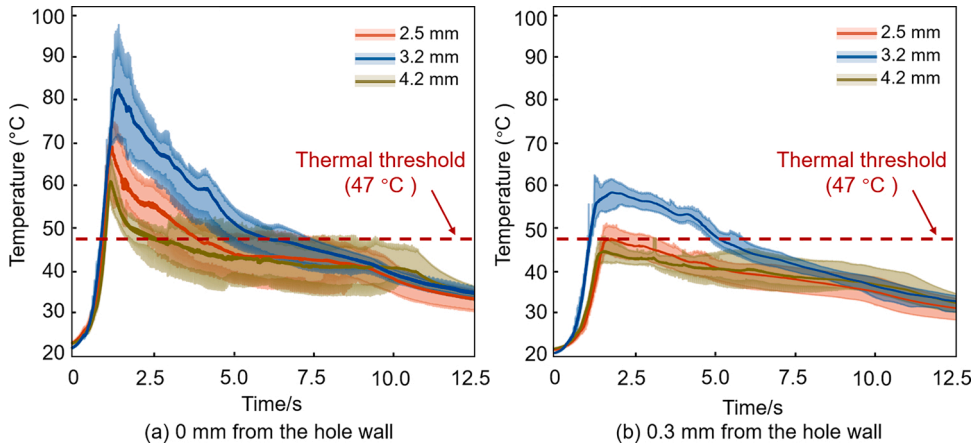

Fig. 11. Effect of drill bit diameter on temperature elevation (perpendicular direction, 1000 rpm, 0.06 mm/rev).

Table 5
Parameter combinations of the feed rate (f), spindle speed (n), and the corresponding outputs (i.e., maximum temperature (T_{max}) and overheat duration (t_{over})) at 0.3 mm from the hole wall.

n (rpm)	f (mm/rev)	Average T_{max} (°C)	RMSE	Average t_{over} (s)	RMSE
500	0.02	61.48	4.27	16.9	1.96
1000	0.02	69.11	2.68	15.1	0.92
1500	0.02	72.3	1.84	15.1	1.42
2000	0.02	76.95	3.16	11.8	1.56
2500	0.02	86.48	3.3	10.8	2.26
500	0.04	57.83	3.55	3.9	1.49
1000	0.04	68.01	2.42	6.4	2.41
1500	0.04	70.65	2.51	7.4	1.32
2000	0.04	74.38	3.75	6.9	0.61
2500	0.04	81	5.28	6.6	0.37
500	0.06	53.72	2.92	3.1	0.87
1000	0.06	65.36	2.37	6.2	1.5
1500	0.06	72.11	3.09	5.7	0.21
2000	0.06	71.79	3.52	4.8	0.88
2500	0.06	77.7	3.17	5	0.43
500	0.08	54.91	4.12	6.1	2.05
1000	0.08	67.14	2.71	5.1	0.69
1500	0.08	71.45	2.64	5.1	0.32
2000	0.08	74.6	2.89	4.4	0.51
2500	0.08	69.64	2.14	3.5	0.46
500	0.1	53.92	3.87	6	1.76
1000	0.1	69.24	2.81	4.5	0.91
1500	0.1	71.77	1.3	4.3	0.22
2000	0.1	73.41	3.12	3.7	0.26
2500	0.1	70.88	5.22	2.5	0.48

in parallel direction drilling. The perpendicular and the transverse direction share the same removal mechanisms that the osteons are perpendicular to the feeding direction. Pulled by the thrust force, the failure of the matrix which bonds the osteons together happened and the last layer of bone was delaminated. The relatively low strength along the transverse direction is thought to be the reason why the delamination and the cracks were more moderate. In parallel direction drilling, the osteons align parallel to the feeding direction, which eliminates the physical basis of delamination. With less dense bone along the feeding direction, only mild micro cracks happened. Considering the mechanical and thermal responses associated with the osteon direction and bone density, the drilling strategy should be carefully selected based on the local bone property. For instance, moderate feed rate should be selected when drilling high strength parts of the bone to avoid excessive mechanical and thermal damage.

The amount of heat generated throughout the entire drilling process increases with the drill bit diameter. The diameter increase leads to a higher ability of chip evacuation and a higher drill bit heat capacity, reducing the heat transferred to the surrounding tissue. Accordingly, in this study, these competing effects resulted in the non-monotonic relationship between the temperature elevation and drill bit diameter; similar results were reported by Bogovič et al. [34]. However, this outcome is contrary to the results of experimental [35] and numerical studies [10], which suggest that the temperature increased with the drill bit diameter. In view of this, further research is required to investigate the competing effects on the relationship between the drill bit diameter and temperature elevation.

Table 6
ANOVA for the maximum temperature elevation (T_{max}).

Source	Sum of Squares	DOF	Mean Square	F-value	p-value	Contribution (%)
Corrected Model	7808.136	24	325.339	23.199	<0.0001	100
n	6494.926	4	1623.732	115.785	<0.0001	89.6
f	565.028	4	141.257	10.073	<0.0001	7.8
$n * f$	744.373	16	46.523	3.317	<0.0001	2.6
Error	1416.397	101	14.024	–	–	–

Table 7
ANOVA for the overheat duration (t_{over}).

Source	Sum of Squares	DOF	Mean Square	F-value	p-value	Contribution (%)
Corrected Model	1870.196	24	77.925	41.087	<0.0001	100
n	67.207	4	16.802	8.859	<0.0001	3.87
f	1622.72	4	405.68	213.898	<0.0001	93.47
$n * f$	183.897	16	11.494	6.06	<0.0001	2.64
Error	191.557	101	1.897	–	–	–

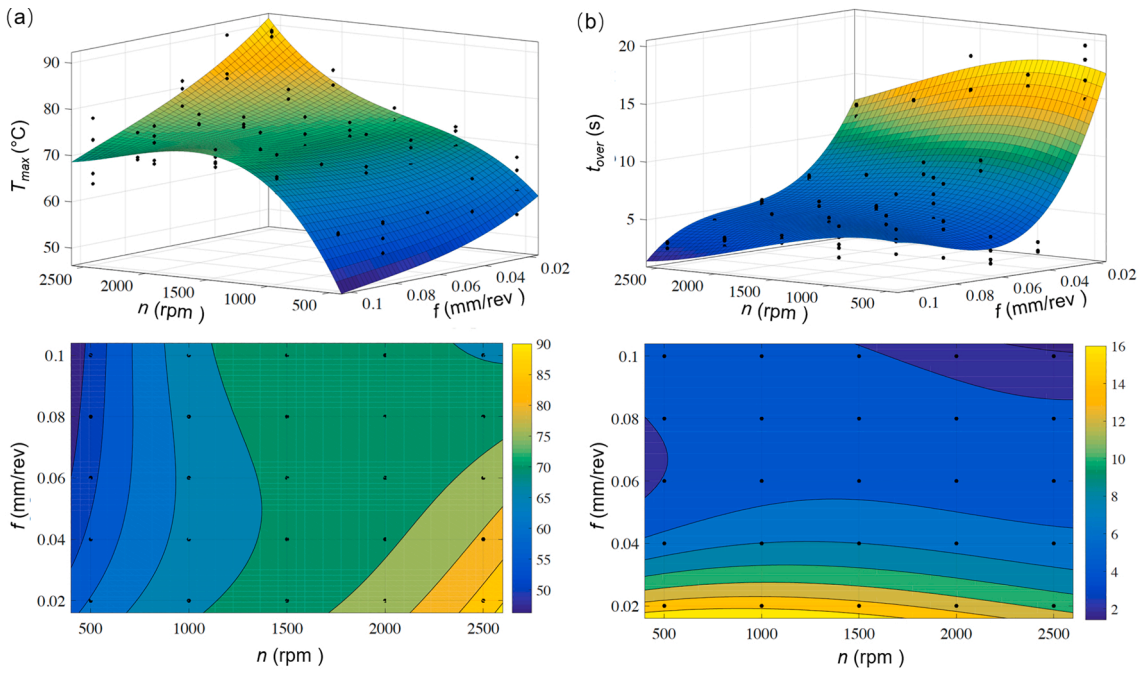

F(*n*, *f*) = p00 + p10**n* + p01* *f* + p20**n* ^2 + p11**n* * *f* + p02* *f* ^2 + p30* *n* ^3 + p21* *n* ^2* *f* + p12* *n* * *f* ^2 + p03* *f* ^3

F(n, f)	p00	p10	p01	p20	p11	p02	p30	p21	p12	p03	R^2
T_{max}	53.6	0.03653	-582.3	-2.32e-05	0.4596	3810	6.086e-9	-0.0001669	-0.08664	-1.355e+04	0.8074
t_{over}	29.5	0.004898	-1085	-5.029e-06	0.1267	1.31e+4	7.409e-10	1.146e-05	-1.313	-4.809e+04	0.9495

Fig. 12. Effect of feed rate (*f*) and spindle speed (*n*) on average maximum temperature (T_{max}) and overheat duration (t_{over}) at 0.3 mm from hole wall with third-order polynomial curve fitting.

To investigate the relationship between processing parameters, T_{max}, t_{over} and the thermal injury, we also calculated the thermally affected zone. The thermally affected zone was calculated based on the equivalent thermal exposure concept [27] and the suggested thermal threshold (47 °C, 60 s) [28]. According to [27], the equivalent thermal exposure for evaluating the thermal damage on a living cell is defined as

$$t_{43} = \int_{t=0}^{t=t_{final}} R(T(t))^{43-T(t)} dt, \text{ where}$$
$$R(T(t)) = \begin{cases} 0.5 & \text{if} T(t) \geq 43°C \\ 0.25 & \text{otherwise,} \end{cases} \quad (1)$$

where t_{43} is the equivalent exposure duration at 43 °C, t_{final} is the exposure duration, $R(T(t))$ is the base at a certain temperature, and $T(t)$ is the temperature at time point t. Four extreme parametric combinations with the longest overheat duration or the highest temperature elevation from Fig. 12 were investigated. The thermally affected zone is shown in Fig. 15. It is obvious that the thermally affected area decreased with the feed rate (i.e., feed per revolution). However, the area decrease was not significant with respect to the spindle speed reduction. According to Fig. 12, we can find that although the t_{over} decreased with the increasing spindle speed, the T_{max} showed an opposite trend. This competing effect may weaken the sensitivity towards spindle speed change. The detail of this competing effect will be further discussed in the next paragraph. Also, it should be noted that the equivalent thermal exposure is a clinical concept. If the equivalent thermal exposure exceeds the range of hundreds of minutes, it will lose practical meaning and can be deemed as an indicator of instantaneous injury. Based on the equation, the bone injury will be sustained in less than 1 s at a temperature exceeding 60 °C, which is consistent with that reported by Shu et al,. [3]. This suggests that the area near the hole wall is more probable to sustain instantaneous injury caused by a high temperature rather than a long thermal exposure duration at a relatively low temperature.

The processing parameters have a significant impact on the temperature elevation and thermal exposure duration in bone drilling. The failure of bone and friction at the tool–bone interface are the two main heat sources in bone drilling. The failure pattern, which depends on the cutting depth, affects the amount of heat generated by the failure of bone. The cutting depth (d_{cut}) is given by

$$d_{cut} = \frac{f_r \cdot \sin(\alpha)}{2} \quad (2)$$

where f_r is the feed per revolution, and α is half the point angle. In this research, the d_{cut} value is in the range of 8.66–43.30 μm. In other words, the overall process is well within the shear-crack cutting range ($d_{cut} < 80$ μm). In this range, the instantaneous heat generation at the tool–bone interface is lower at a smaller d_{cut} value; while the overall heat generation for removing a certain volume of bone is lower at a higher d_{cut} value [36]. Considering the linear relationship between d_{cut} and f_r, it is concluded that a higher f_r leads to a higher maximum temperature at the cutting lips but a lower overall heat generation throughout the process. Meanwhile, at a certain f_r value, a higher spindle speed leads to a higher frictional heat generation per unit time [7,24,37], while the total processing time was reduced because of the increase in the feed per unit time induced by higher spindle speed. Those competing effects made it difficult to determine the relationship between processing parameters and the thermal dose. To address this issue, we have investigated the effect of processing parameters on thermal characteristics. As shown in Fig. 12, T_{max} and t_{over} present a declining trend with increasing f_r. Meanwhile, t_{over} decreases as the spindle speed increases, T_{max} however shows an opposite trend. Another important information is that the contribution was different according to the Tables 6 and 7—the spindle speed and the feed rate (feed per revolution) contributed to T_{max} and t_{over} the most, respectively. We can infer from the results presented above that if the f_r decreases, there would be a major reduction in t_{over} and a

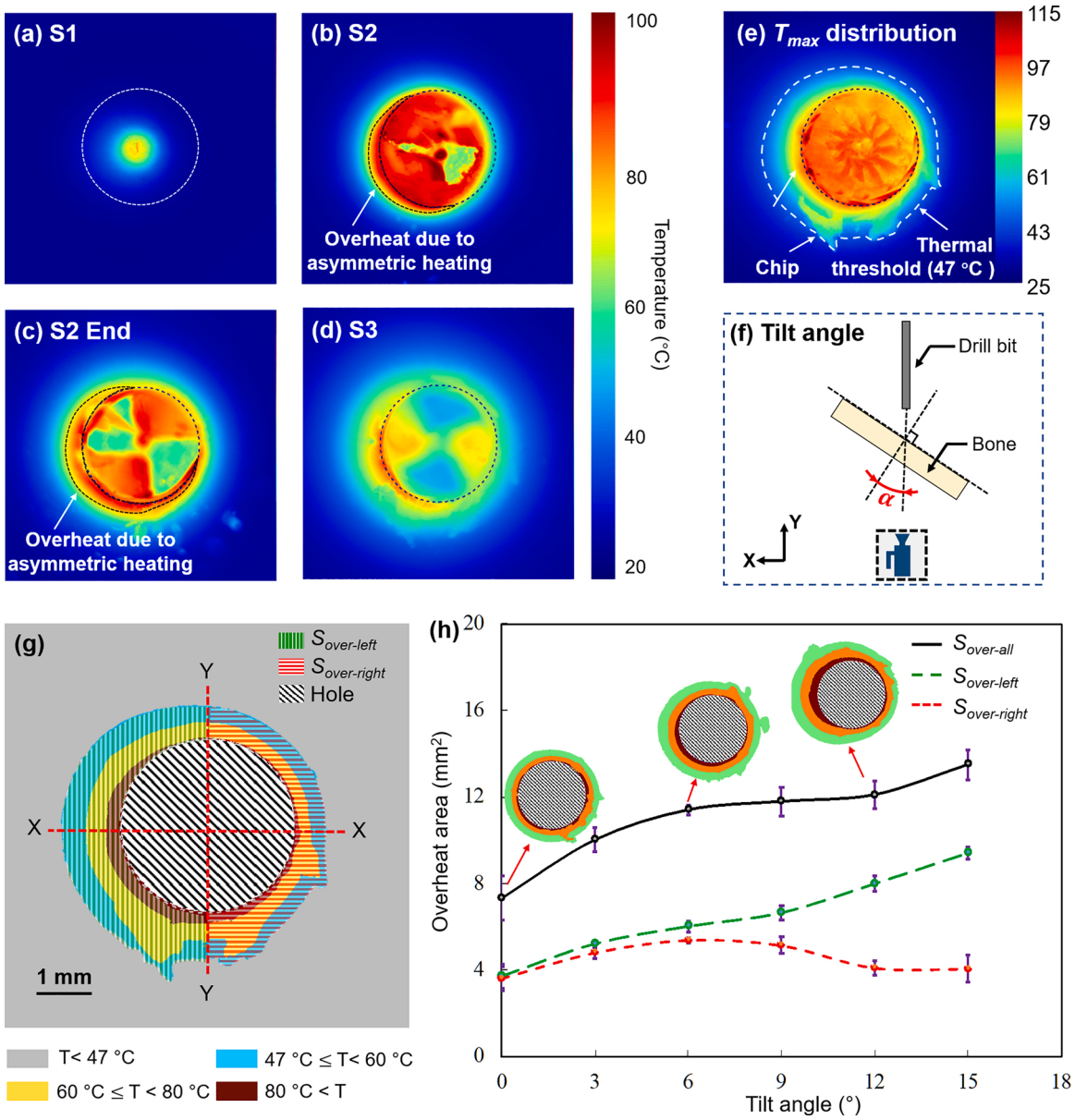

Fig. 13. Effect of tilt angle on thermal characteristics and overheat area during non-perpendicular bone drilling. (a–e) Time series temperature distribution, (f) maximum temperature distribution, (g) overheat zone in 9° inclined drilling, and (h) variation of overheat area with the tilt angle. (1000 rpm, 0.06 mm/rev).

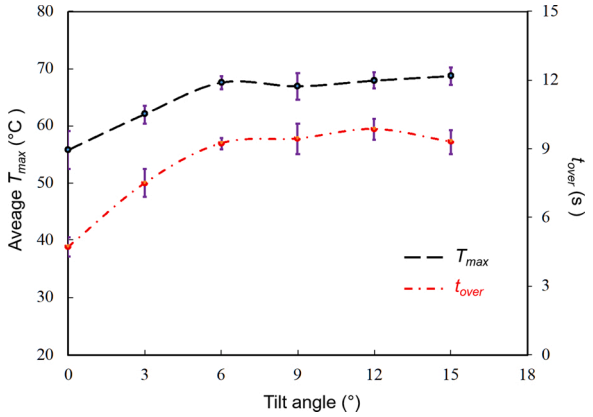

Fig. 14. Effect of tilt angle on average maximum temperature (T_{max}) and overheat duration (t_{over}) at a distance of 0.3 mm from the hole wall. (1000 rpm, 0.06 mm/rev).

minor reduction in T_{max}; moreover, if the spindle speed decreases, there would be a major increase in T_{max} and a minor decrease in t_{over}. The competing effects of the T_{max} and t_{over} on the thermally affected zone (Fig. 15) can thus be explained—the thermally affected area decreased significantly with the increasing f_r because both the T_{max} and t_{over} decreased; meanwhile, there was only minor decrease in the thermally affected area with increasing spindle speed because the major increase in T_{max} and a minor decrease in t_{over}. These results suggest that although there are competing effects between the feed rate and spindle speed, the process duration may be the governing factor that finally determines the overall thermal dose, which was also reported by several experimental studies [12,38,39]. Another interesting finding is that there are actually two strategies at a certain f_r value: one is the application of a higher spindle speed to achieve a lower t_{over}, and the other is the application of a lower spindle speed to achieve a lower T_{max}.

There are some limitations of this research. Firstly, the cooling effect of soft tissue and body fluid underneath the cortical bone, and the cooling induced by irrigation technique are not considered. Both two types of interactions help to reduce the local temperature rise in the

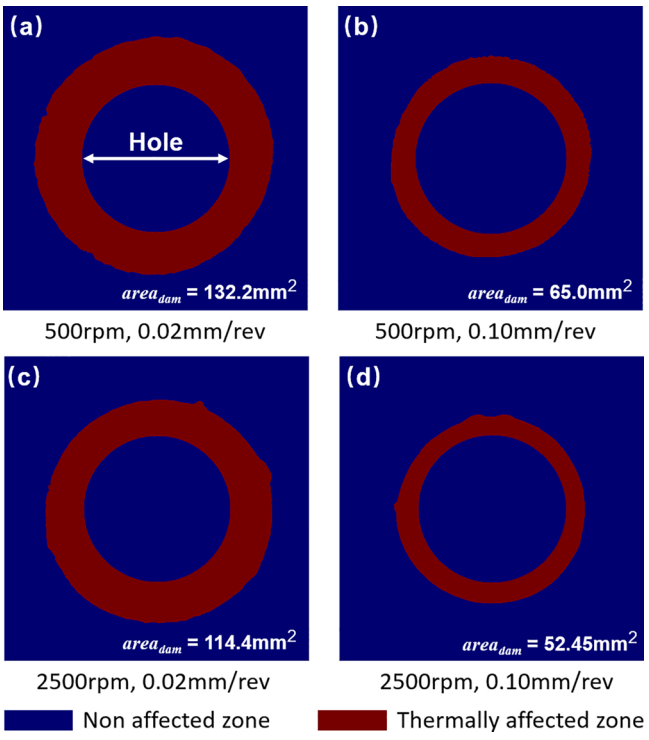

Fig. 15. Thermally affected zone of bone under four critical drilling conditions in the experiment.

cortical bone around the drilling site by means of absorbing and dissipating the heat. However, the cooling effects of these two interactions are limited in drilling deep holes on cortical bone [4,20]. Karmani et al. concluded that the coolant could hardly reach the tool-bone interface when drilling deep into the cortical bone and only the superficial tissue can be cooled. Also, from the experimental results of Eriksson et al., we can find that the in-vivo human bone drilling (irrigation applied) ended up with a local temperature up to 89 °C. Note that the coolant cannot reach deep into the hole. This means the temperature reached 89 °C during bone drilling when the soft tissue and body fluid acted as the only coolant. Hence, the influence of not considering the two cooling effects in this research is deemed to be limited. Secondly, the thermal injury of bone tissue was not assessed through the biological indicator. Although the thermally affected zone of 4 parametric combinations based on the equivalent thermal exposure concept [27] and the suggested thermal threshold (47 °C, 60 s) [28] was calculated, a further biological investigation is still needed. Future studies are required to further reveal the direct relevance between thermal injury and the thermal characteristics during bone drilling. Histopathological assessment [40] and immunohistochemistry staining [29] methods, which were applied in the previous studies, are suggested to be conducted together with the methods proposed in this research. Thus, a direct relationship between the thermal injury and the thermal characteristics during bone drilling may be revealed through investigation on the 3-dimensional thermal injury area and the time-series temperature distribution.

5. Conclusions

The thermal characteristics during bone drilling directly affect the thermal damage of the bone and perform a critical role in the post-operative recovery. In this study, a comprehensive experimental investigation was conducted to understand the thermal characteristics during cortical bone drilling using a bone cutting system coupled with the state-of-the-art infrared thermography and dynamometer. The conclusions drawn are summarized as follows:

(1) Three typical stages were defined with respect to the heat source. In the chisel edge cutting stage, the bone outside of the hole was practically unaffected even with considerable heat generation. The heat generated in the chisel edge cutting stage forms the temperature base of the drilling process. In the lip cutting stage, a considerable amount of heat was generated by the failure of bone (termed shear-crack cutting in this study), leading to the maximum temperature elevation of the bone in the vicinity of the hole wall. In the margin friction stage, the heat generated by the friction between the margin and bone became the main heat source. The maximum temperature and exposure duration are most affected by the lip cutting and margin friction stages, respectively; these determine the thermal dose near the drilling site.

(2) The time series temperature distribution, temperature history at different distances, and quasi-3D maximum temperature distribution were established and analyzed. Under each of the three feeding directions, no sign of anisotropy on the temperature distribution was observed, and T_{max} and t_{over} exhibited differences mainly because of the different removal mechanisms and bone densities. The temperature elevation considerably depends on the distance from the hole wall, and the thermally affected zone can spread up to 0.5 mm from the hole wall.

(3) The processing parameters have a significant impact on the temperature elevation and thermal exposure duration in bone drilling. Both the maximum temperature and overheat duration presented a declining trend with the feed rate (i.e., feed per revolution). The overheat duration decreased at an increased spindle speed, whereas the maximum temperature increased with the spindle speed. Overall, the duration of the drilling process may be the governing factor that can finally determine the thermal dose.

(4) The temperature distribution in inclined drilling exhibited a strong directionality as a result of the asymmetric friction induced by the lateral force. The temperature elevation and overheating duration were higher than those in perpendicular drilling, and the thermally affected zone increased with the tilt angle.

This is the first study to reveal the thermal characteristics at the drill exit in full detail with respect to the bone properties, processing parameters, drill-bit geometries, and inclined drilling. These results provide a fundamental understanding of the parameters affecting thermal effects in bone drilling and subsequently contribute to the formulation of various strategies for reducing the thermal damage during bone drilling.

Funding

Supported by the Open Research Fund of State Key Laboratory of Digital Manufacturing Equipment and Technology,Huazhong University of Science and Technology (No. DMETKF2020004) and National Natural Science Foundation of China (Grant No. 52005199).

Declaration of Competing Interest

The authors report no declarations of interest.

Acknowledgments

The authors express their gratitude to Ms. Koarai Aki and Mr. Matsui Motoomi of Nippon Avionics Co., Ltd. for their advice and inputs regarding temperature in the conduct of the experiment. The authors would also thank the discussion of statistical analysis from Prof. Jianbo Sui from the Guangdong University of Technology.

References

[1] Xi L, Wen W, Wu W, Qu Z, Tao R, Karunaratne A, et al. Mechanical response of cortical bone in compression and tension at the mineralized fibrillar level in steroid induced osteoporosis. Compos Part B Eng 2020:196. https://doi.org/10.1016/j.compositesb.2020.108138.

[2] Hillery MT, Shuaib I. Temperature effects in the drilling of human and bovine bone. J Mater Process Technol 1999;93:302–8.

[3] Shu L, Li S, Ying Z, Sugita N. Thermographic assessment of heat-induced cellular damage during orthopedic surgery. Med Eng Phys 2020. https://doi.org/10.1016/j.medengphy.2020.05.014.

[4] Eriksson AR, Albrektsson T, Albrektsson B, Albrekt T. Heat caused by drilling cortical bone: temperature measured in vivo in patients and animals. Acta Orthop 1984;55:629–31. https://doi.org/10.3109/17453678408992410.

[5] Kalidindi V. Optimization of drill design and coolant systems during dental implant surgery. 2004.

[6] Tu YK, Chen LW, Ciou JS, Hsiao CK, Chen YC. Finite element simulations of bone temperature rise during bone drilling based on a bone analog. J Med Biol Eng 2013;33:269–74. https://doi.org/10.5405/jmbe.1366.

[7] Sezek S, Aksakal B, Karaca F. Influence of drill parameters on bone temperature and necrosis: a FEM modelling and in vitro experiments. Comput Mater Sci 2012;60:13–8. https://doi.org/10.1016/j.commatsci.2012.03.012.

[8] Fernandes MG, Fonseca EM, Jorge RN. Thermo-mechanical stresses distribution on bone drilling: numerical and experimental procedures. Proc Inst Mech Eng Part L J Mater Des Appl 2019;233:637–46. https://doi.org/10.1177/1464420716689337.

[9] Sui J, Sugita N, Mitsuishi M. Thermal modeling of temperature rise for bone drilling with experimental validation. J Manuf Sci Eng Trans ASME 2015;137:1–10. https://doi.org/10.1115/1.4030880.

[10] Lee J, Rabin Y, Ozdoganlar OB. A new thermal model for bone drilling with applications to orthopaedic surgery. Med Eng Phys 2011;33:1234–44. https://doi.org/10.1016/j.medengphy.2011.05.014.

[11] Karaca F, Aksakal B, Kom M. Influence of orthopaedic drilling parameters on temperature and histopathology of bovine tibia: an in vitro study. Med Eng Phys 2011;33:1221–7. https://doi.org/10.1016/j.medengphy.2011.05.013.

[12] Sharawy M, Misch CE, Weller N, Tehemar S. Heat generation during implant drilling: the significance of motor speed. J Oral Maxillofac Surg 2002;60:1160–9. https://doi.org/10.1053/joms.2002.34992.

[13] Soler D, Aristimuño PX, Esnaola JA, Arrazola PJ. Determining tool / chip temperatures from thermography measurements in metal cutting. Appl Therm Eng 2018;145:305–14. https://doi.org/10.1016/j.applthermaleng.2018.09.051.

[14] Merino-pérez JL, Royer R, Ayvar-soberanis S, Merson E, Hodzic A. On the temperatures developed in CFRP drilling using uncoated WC-Co tools Part I: workpiece constituents, cutting speed and heat dissipation. Compos Struct 2015;123:161–8. https://doi.org/10.1016/j.compstruct.2014.12.033.

[15] Bertollo N, HRMM Milne, Ellis LP, Stephens PC, Gillies RM, Walsh WR. A comparison of the thermal properties of 2- and 3-fluted drills and the effects on bone cell viability and screw pull-out strength in an ovine model. Clin Biomech (Bristol, Avon) 2010;25:613–7. https://doi.org/10.1016/j.clinbiomech.2010.02.007.

[16] Vaughan TJ, Niebur GL, Casey C, Tallon D, Dolan EB, Vaughan TJ, et al. How bone tissue and cells experience elevated temperatures during orthopaedic cutting: an experimental and computational investigation. J Biomech Eng 2014;136:021019. https://doi.org/10.1115/1.4026177.

[17] Sugita N, Ishii K, Sui J, Terashima M. Multi-grooved cutting tool to reduce cutting force and temperature during bone machining. CIRP Ann Manuf Technol 2014;63:101–4. https://doi.org/10.1016/j.cirp.2014.03.069.

[18] Fernandes MG, Fonseca EMM, Jorge RN, Vaz M, Dias MI. Thermal analysis in drilling of ex vivo bovine bones. J Mech Med Biol 2017;17:1–16. https://doi.org/10.1142/S0219519417500828.

[19] Fernandes MGA, Fonseca EMM, Natal RJ. Thermal analysis during bone drilling using rigid polyurethane foams: numerical and experimental methodologies. J Brazilian Soc Mech Sci Eng 2016;38:1855–63. https://doi.org/10.1007/s40430-016-0560-4.

[20] Karmani S. The thermal properties of bone and the effects of surgical intervention. Curr Orthop 2006;20:52–8. https://doi.org/10.1016/j.cuor.2005.09.011.

[21] Shu L, Li S, Terashima M, Bai W, Hanami T, Hasegawa R, et al. A novel self-centring drill bit design for low-trauma bone drilling. Int J Mach Tools Manuf 2020;154:103568. https://doi.org/10.1016/j.ijmachtools.2020.103568.

[22] Feldmann A, Wili P, Maquer G, Zysset P. The thermal conductivity of cortical and cancellous bone. Eur Cells Mater 2018;35:25–33. https://doi.org/10.22203/eCM.v035a03.

[23] Jung YG, Choi SC, Oh CS, Paik UG. Residual stress and thermal properties of zirconia/metal (nickel, stainless steel 304) functionally graded materials fabricated by hot pressing. J Mater Sci 1997;32:3841–50. https://doi.org/10.1023/A:1018640126751.

[24] Lee JE, Ozdoganlar OB, Rabin Y. An experimental investigation on thermal exposure during bone drilling. Med Eng Phys 2012;34:1510–20. https://doi.org/10.1016/j.medengphy.2012.03.002.

[25] Liao Z, Axinte DA. On chip formation mechanism in orthogonal cutting of bone. Int J Mach Tools Manuf 2016;102:41–55. https://doi.org/10.1016/j.ijmachtools.2015.12.004.

[26] Yuen H, Princen J, Illingworth J, Kittler J. Comparative study of Hough Transform methods for circle finding. Image Vis Comput 1990;8:71–7. https://doi.org/10.1016/0262-8856(90)90059-E.

[27] Sapareto SA, Dewey WC. Thermal dose determination in cancer therapy. Int J Radiat Oncol Biol Phys 1984;10:787–800. https://doi.org/10.1016/0360-3016(84)90379-1.

[28] Eriksson RA, Albrektsson T. The effect of heat on bone regeneration. J Oral Maxillofac Surg 1984:705–11.

[29] Dolan EB, Tallon D, Cheung WY, Schaffler MB, Kennedy OD, Mcnamara LM. Thermally induced osteocyte damage initiates pro-osteoclastogenic gene expression in vivo. J R Soc Interface 2016:13. https://doi.org/10.1098/rsif.2016.0337.

[30] Feldmann A, Anso J, Bell B, Williamson T, Gavaghan K, Gerber N, et al. Temperature prediction model for bone drilling based on density distribution and in vivo experiments for minimally invasive robotic cochlear implantation. Ann Biomed Eng 2016;44:1576–86. https://doi.org/10.1007/s10439-015-1450-0.

[31] Zhang Y, Xu L, Wang C, Chen Z, Han S, Chen B, et al. Mechanical and thermal damage in cortical bone drilling in vivo. Arch Proc Inst Mech Eng Part H J Eng Med 1989-1996 2019;233:621–35. https://doi.org/10.1177/0954411919840194.

[32] Sui J, Wang C, Sugita N. Experimental study of temperature rise during bone drilling process. Med Eng Phys 2020;78:64–73. https://doi.org/10.1016/j.medengphy.2020.01.007.

[33] Bensamoun S, Ba MH, Luu S, Gherbezza JM, Ho Ba Tho MC, Luu S, et al. Spatial distribution of acoustic and elastic properties of human femoral cortical bone. J Biomech 2004;37:503–10. https://doi.org/10.1016/j.jbiomech.2003.09.013.

[34] Bogović V, Svete A, Bajsić I. Effects of a drill diameter on the temperature rise in a bone during implant site preparation under clinical conditions. Arch Proc Inst Mech Eng Part H J Eng Med 1989-1996 2016;230:907–17. https://doi.org/10.1177/0954411916660737.

[35] Augustin G, Davila S, Mihoci K, Udiljak T, Stjepan D, Anko V, et al. Thermal osteonecrosis and bone drilling parameters revisited. Arch Orthop Trauma Surg 2008;128:71–7. https://doi.org/10.1007/s00402-007-0427-3.

[36] Feldmann A, Ganser P, Nolte L, Zysset P. Orthogonal cutting of cortical bone: temperature elevation and fracture toughness. Int J Mach Tools Manuf 2017;118–119:1–11. https://doi.org/10.1016/j.ijmachtools.2017.03.009.

[37] Augustin G, Zigman T, Davila S, Udilljak T, Staroveski T, Brezak D, et al. Cortical bone drilling and thermal osteonecrosis. Clin Biomech (Bristol, Avon) 2012;27:313–25. https://doi.org/10.1016/j.clinbiomech.2011.10.010.

[38] Kondo S, Okada Y, Iseki H, Hori T, Takakura K, Kobayashi A, et al. Thermological study of drilling bone tissue with a high-speed drill. Neurosurgery 2000;46:1162–8. https://doi.org/10.1097/00006123-200005000-00029.

[39] Soriano J, Garay A, Aristimuño P, Iriarte LM, Eguren JA, Arrazola PJ, et al. Effects of rotational speed, feed rate and tool type on temperatures and cutting forces when drilling bovine cortical bone. Mach Sci Technol 2013;17:611–36. https://doi.org/10.1080/10910344.2013.837353.

[40] Kanaya H, Enokida M, Uehara K, Ueki M, Nagashima H. Thermal damage of osteocytes during pig bone drilling: an in vivo comparative study of currently available and modified drills. Arch Orthop Trauma Surg 2019. https://doi.org/10.1007/s00402-019-03239-y.